I.J. Wireless and Microwave Technologies, **2023, 3, 26-38**
Published Online on June 8, 2023 by MECS Press (http://www.mecs-press.org/)
DOI: 10.5815/ijwmt.2023.03.03

Full-Wave Numerical Analysis of Dual-Band E-Patch Antenna and Reactive Loading Technique to Ascertain the Impedance Driving Point Function

Fubara Edmund Alfred-Abam*
Bells University of Technology, Department of Electrical & Electronics Engineering, Nigeria
Email: abamfubara@yahoo.com
ORCID iD: https://orcid.org/0000-0003-4574-0654
*Corresponding Author

Pam Paul Gyang
University of Lagos, Department of Electrical & Electronics Engineering, Nigeria
Email: gyangpaulpam@gmail.com
ORCID iD: https://orcid.org/0000-0001-9041-4490

Fiyinfoluwa P. Olubodun
Federal University of Technology, Department of Electrical & Electronics Engineering, Nigeria
Email: ofpelumi@gmail.com
ORCID iD: https://orcid.org/0000-0001-7985-1892

Received: 06 October, 2022; Revised: 20 November, 2022; Accepted: 24 December, 2022; Published: 08 June, 2023

Abstract: This paper encompasses the numerical analysis involved with the Electromagnetic (EM) full-wave simulation tool Advanced Design System (ADS) which uses the Method of Moment (MOM) and Finite Element Method (FEM). MOM is utilized to solve Maxwell's equations which are transformed into integral equations before discretization and boundary conditions are applied while FEM computes the electrical behavior of the high frequency EM wave distribution, and then analyze the antenna parameters. The main objective is to investigate the effect of reactive loading on the microstrip patch surface which is used to control the behavior of the impedance bandwidth and obtain dual-band frequency operation. The study further examines how the perturbed patch antenna design targets the operating frequencies of 2.4 GHz and 5.8 GHz for possible range and speed. The proposed method provides insight into the analysis of the mathematical model employed in attaining the Driving Point Impedance Function (DPF) of the E-patch microstrip patch antenna. This approach was done to quantify the reduction in reflections for improved Radio Frequency (RF) network output.

Index Terms: Driving Point Function, Dual Band, Finite Element Method, Input Impedance, Method of Moment, Microstrip Patch Antenna, Reactive Loading.

1. Introduction

Microstrip patch antennas have become attractive planar candidates in varieties of commercial applications such as satellite and mobile communication. Microstrip antennas are capable of single and multiple frequency operation and are mechanically robust when mounted on a rigid surface [1]. Microstrip patch antennas can be reconfigured based on their mode of operation and shape selection, designs can then become versatile depending on the application requirement [2]. Although patch antennas are advantageous, however, they exhibit substantial drawbacks such as narrow impedance bandwidth, low-power handling capacity, low gain, poor polarization purity, spurious feed radiation, and the associated manufacturing tolerance issues [3]. These problems are mostly inherent based the patch antenna shape, size and relative permittivity of the substrate.

The microstrip antenna consists of two thin metallic layers separated by a dielectric substrate, with one layer as the radiating patch, and the other as the ground plane [4]. The radiating element is the conductor patch found on top of the dielectric substrate, while a conductive layer is also used as the ground plane, which is found on the other end of the substrate. Several materials such as copper, gold, or aluminum are used as metallic layers and varieties of dielectric materials ranging from $2.2 \leq \varepsilon_r \geq 12$ are available for designing MSA.

The substrate height plays a vital role in antenna characteristics such as producing narrow frequency bandwidths, which are not entirely appreciated for numerous applications. The MSA bandwidth is directly proportional to the height of the substrate and several methods can be employed to improve the bandwidth. Also, the characteristics of the antenna do not solely depend on the antenna elements but are influenced by the transmission line when combined with the antenna. Usually, the input impedance of the MSA is complex, while the characteristic impedance is real and generally 50 Ω. With this, impedance matching becomes tough; causing voltage standing waves on the transmission line, and then resulting in low impedance bandwidth [3].

The radiation mechanism of a patch antenna demonstrates the cause of the challenge that results in the fringing effect with respect to the voltage and current relationship on the antenna. The patch antennas are half-wavelength long and are terminated in an open-circuit with the current at maximum or peak at the center of the patch, and the voltage zero at the center of the patch. This generally implies that the current and voltage will be 90 degrees out of phase. The voltage is maximum positive at the beginning of the patch and minimum negative at the end of the patch, while the current is maximum at the center of the patch and zero at both the beginning and the end of the patch. Impedance matching can be achieved since the impedance distribution is maximum at both the patch edges and minimum at the center. Therefore, there will be a point which lies on the surface of the radiating patch where the impedance will be 50 Ω. Hence an iterative approach can be applied to locate the position of 50 Ω using coaxial probe feed [5].

Figure 1 shows the relationship of the current (I), voltage (V), and impedance (Z) on an open-end microstrip patch. The current is maximum at the center of the patch and minimum at the edge of the parallel plate. However, the voltage is maximum positive at one end and minimum negative at the other end, but minimum at the center of the patch plate. The impedance is the ratio of V to I on the patch and this suggests a possible suitable point for matching these antenna types.

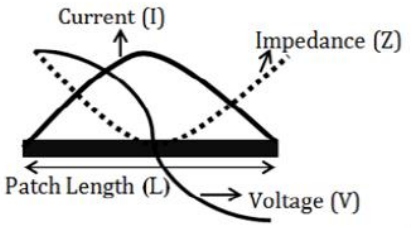

Fig. 1. Current, Voltage and Impedance variation along the patch length.

For an antenna to radiate, either the current or the voltage is added up in phase. The patch acts as a parallel plate microstrip transmission line, where is wavelength in the dielectric medium. The fringing fields are responsible for radiation and exist at the edge of the parallel plate [6].

These fields are in the same direction, and this is due to the Rectangular Microstrip Patch Antenna (RMSA) current and voltage not adding up in phase but canceling out each other. This leads to field distribution on the patch antenna with the field not abruptly stopping at the patch end but creating a horizontal component adding up in phase. These are known as the fringing fields, which are the reasons behind the microstrip patch antenna radiation [7]. Figure 2 shows the side view of the patch antenna with the E-fields shown underneath. Since fringing fields are both in the +y direction, the fringing E-fields at the patch end add up in phase giving rise to radiation.

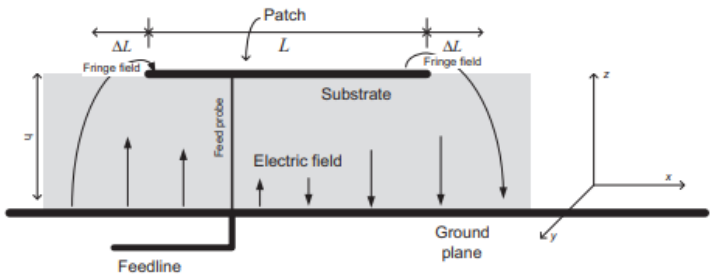

Fig. 2. Fringing field effect.

2. Literature Review

a) Full-wave Numerical Analysis

The Advanced Design System (ADS) converts the design into a mesh and computes a number of segmentation based on the size of the design. After the segmentations, the ADS helps in calculating the EM wave distributions and then compute the radiation pattern, impedance, return loss, and the VSWR. The ADS uses the Method of Moment (MOM), along with the Finite Element Method (FEM).

The ADS CAD uses MOM to solve Maxwell's equations which are transformed into integral equations before discretization and boundary conditions are applied while FEM is used to generate the Electromagnetic Field (EMF) solution from which the scattering parameters can be computed. The FEM splits the problem space into thousands of regions by representing the EMF in every single element with a local function. During the simulation, the FEM divides a geometric model automatically into a large number of tetrahedral, formed by four equilateral triangles, wherever a single tetrahedron is found. A value of the vector field quantity (H-field or E-field) at a specific location inside each tetrahedron is interpolated from the vertices of the tetrahedron.

Once a mesh has been created, some basis functions are then defined for each tetrahedron. The basis function, W_n, defines the condition concerning the nodal location in the general mesh of the tetrahedral, based on the input problem. The accuracy of the solutions depends on a number of individual elements present; also, every single tetrahedron needs to occupy a region that is small enough for the field to be sufficiently interpolated from the nodal values [2]. The basis functions are multiplied by the field equation, which conforms to Maxwell's relation according to Eq. (1).

$$\nabla \times \left(\frac{1}{\mu_r} + \vec{E} \right) - K_0^2 \varepsilon_r \vec{E} = 0 \tag{1}$$

The outcome of the basis function W_n multiplied by the field equation where, μ_r, $\vec{E}$, K_0 and ε_r are relative permeability, vector wave equation, free space wave number and relative permittivity as represented by Eq. (2).

$$\int_v \left[W_n . \nabla \times \left(\frac{1}{\mu_r} + \vec{E} \right) - K_0^2 \varepsilon_r \vec{E} \right] dV = 0 \tag{2}$$

The resulting Eq. (2) is then written using Greens function and divergence theorem and equated to excitation boundary terms, according to Eq. (3):

$$\int_v \left[(\nabla \times W_n) . \left(\frac{1}{\mu_r} + \vec{E} \right) - K_0^2 \varepsilon_r \vec{E} \right] dV = \int_v boundary\, term \tag{3}$$

The electric field vector $\vec{E}$ can now be expressed as a summation of unknown complex coefficients, I_m multiplied by the current on the object using the same basis function that was employed to generate an initial series equation W_m, as described by Eq. (4) [2]:

$$\vec{E} = \sum_{m=1}^{N} I_m W_m \tag{4}$$

The basis functions can be useful over a limited range of a piecewise linear function structure, which can be a sinusoidal or triangular in nature according to Eq. (5).

$$\sum_{m=1}^{N} I_m . \left(\int_v \left[(\nabla \times W_n) . \left(\frac{1}{\mu_r} + W_m \right) - K_0^2 \varepsilon_r W_n W_m \right] dV \right) = \int_s (boundary\, term) dS \tag{5}$$

Hence, the resulting equations do permit the solution of the unknown coefficients I_m, to find the electric fields on a Perfect Electric Conductor (PEC) surface. When the value has been calculated using the solver, the entire process can be carried out for a second adaptive pass. The matrix equation is obtained using the unit current on each basis function, suppose that a linear equation is considered, as represented by Eq. (6).

$$L(W) = f \tag{6}$$

Where L is the linear operator transfer function, W is the unknown function to be determined and f is the excitation function representing the source. The objective is to determine W once L and f are specified. The solution is determined by the summation of unknown complex coefficients, I_m: m = 1, 2…M multiplied by the current on the object using the same basis function employed to generate the initial series equation W_m: W_1, W_2, W_3…. in the domain operator of a linear function. In effect, this is achieved by expanding the function W using a series of the known basis functions given by Eq. (7):

$$W = \sum_m I_m W_m \tag{7}$$

Furthermore, the expanding function, W is replaced in Eq. (6) by Eq. (7) with the linearity of L in use; this leads to Eq. (8):

$$W = \sum_m I_m L(W_m) = f \tag{8}$$

The issue now becomes how to determine the unknown coefficients I_m. Hence, a second set of weighting or testing functions, N_n: N_1, N_2, N_3… is chosen in the L domain to form an inner product where n = 1, 2…N according to Eq. (9).

$$\sum_m I_m \{N_n, L(W_m)\} = \{N_n, f\} \tag{9}$$

The inner product of Eq. (9) is performed for n = 1 to N to give the matrix described by Eq. (10) [2]:

$$\begin{pmatrix} & & \\ < N_1.L(W_1) > & < N_1.L(W_2) > & < N_1.L(W_m) > \\ < N_2.L(W_1) > & < N_2.L(W_2) > & < N_2.L(W_m) > \\ \cdots & \cdot & \cdot \\ < N_n.L(W_n) > & \cdots & < N_n.L(W_m) > \end{pmatrix} \begin{pmatrix} I_1 \\ I_2 \\ \cdot \\ I_m \end{pmatrix} = \begin{pmatrix} < N_1.f > \\ < N_2.f > \\ \cdot \\ < N_n.f > \end{pmatrix} \tag{10}$$

Or the matrix equation can be expressed in a more compact form according to Eq. (11):

$$[Z_{mn}][I_m] = [V_n] \tag{11}$$

This leads to the definition of important parameters, as presented in Eqs. (12), (13) and (14) [2]:

$$Z_{mn} = < N_n.L(W_1) > \tag{12}$$

$$V_n = < N_n.f > \tag{13}$$

$$[I_m] = [Z_{mn}]^{-1}[V_n] \tag{14}$$

Hence, the unknown function W can be approximately obtained using Eqs. (7) and (19). From Eq. (11), it is possible to generalize the eigenvalue problem considering the operator Z as described by Eq. (15):

$$(Z)(j_n) = v_n(W)(j_n) \tag{15}$$

The eigenvector $[j_n]$ can then be considered as the eigen currents for the conducting surface defined by the impedance operator Z. From this point, the boundary condition on the PEC surface can now be enforced by Greens function expressed in Eq. (3), and the general impedance operator Z according to Eq. (16).

$$Z(\overrightarrow{J_s}) = R(\overrightarrow{J_s}) + jX(\overrightarrow{J_s}) \tag{16}$$

Where j_s characterizes the patch surface current and the Poynting function output is a ratio of P_{stored} to P_{rad} given by Eq. (17) [10]:

$$F(\overrightarrow{J_s}) = \frac{X(\overrightarrow{J_s}).(\overrightarrow{J_s}^*)}{R(\overrightarrow{J_s}).(\overrightarrow{J_s}^*)} = \frac{P_{stored}}{P_{rad}} \tag{17}$$

From Eq. (14), the general expression for the eigenvalue is obtained; it is then linked with the Lagrange multipliers according to Eq. (18):

$$X(\overrightarrow{J_s}n) = \lambda_n R(\overrightarrow{J_s}n) \tag{18}$$

In order to solve for the eigenvectors and eigenvalues, the process of discretization of the operator Z is carried out. The matrix form of the eigenvalue is represented by Eq. (19):

$$[X - \lambda_n R][\overrightarrow{j_n}] = 0 \tag{19}$$

From this point, several steps are omitted for brevity following the Foster reactance theorem and antenna Q. Here, W = w_e or w_m which stands for total stored electric or magnetic energy in the volume surrounding the radiator as given by Eq. (20) to (22) [10].

$$Q_n = \frac{2\omega W_{,n}}{P_{rad,n}} \tag{20}$$

$$Q_n = 2\omega \frac{\max(W_{e,n,}W_{m,n})}{P_{rad,n}} \tag{21}$$

$$Q_n = \frac{[I_n^*]\left[\omega\left(\frac{dX_n}{d\omega}\right) \pm X_n\right][I_n]}{[I_n^*]\left[[Z_A]+[Z_A^*]\right][I_n]} \tag{22}$$

Hence, it is possible to replace λ_n in the expression for Q_n as presented in Eq. (23):

$$= Q_n = \frac{[I_n^*]\left[\omega\left(\frac{d\lambda_n}{d\omega}\right) \pm \lambda_n\right][I_n]}{[I_n^*]\left[[Z_A]+[Z_A^*]\right][I_n]} \tag{23}$$

By replacing this term means that the current mode is frequency-dependent; also, the n^{th} eigenvalue of λ_n is related to Q_n and the bandwidth BW_n as given by Eq. (24):

$$\left[BW_n \propto \frac{1}{Q_n}\right] \tag{24}$$

This relationship determines how small or big the fractional bandwidth is at a specific antenna frequency if the associated value of Q_n is low or high.

b) Related works

This aspect presents the review of existing research works concerning the microstrip patch antenna. Quite a few authors reported different methods and contributions, which form a good background for this paper. For instance, a compact rectangular slot patch antenna for dual-frequency operation using the inset feet technique was presented [11]. The authors focused on miniaturized antenna design having a size of 44 x 41 x 1.6 mm^3. The microstrip feed line method was used in conjunction with standard mathematical models, employed to identify the input impedance point. The approach involved the use of full-wave simulation, and the result showed a return loss of – 19.6 dB and a VSWR of 1.303 at 2.4 GHz, with – 17.5 dB and 1.301 at 5.2 GHz applicable to WLAN and Bluetooth technology. In another

paper, A compact design and simulation of rectangular multiband and ultra-wideband microstrip patch antenna with circular polarization has also been presented [12]. The design focused on achieving an ultra-wideband with less noise interference for applications in wireless local area network and satellite communication represented by S, C and X bands. The antenna resonates primarily in S, C, and X frequency band regions having notches at 2.6 GHz, 5.0 GHz, 6.5 GHz, and 10.8 GHz. The return loss is approximately less than – 10 dB for a large band characterized as an ultra-wideband antenna.

Also, the modeling and simulation of a rectangular microstrip antenna was presented [13]. This paper looks into the problem of single patch antenna low gain using a Matlab working environment. Basically, different dielectric constants were analyzed for 3 different antennas to identify the maximum gain and best return loss. In this study, the Transmission Line Model (TLM) and cavity models were used to analyze the Rectangular Microstrip Patch Antenna (RMSA). The 3 different antennas operate at 10 GHz, 2.40 GHz and 2.25 GHz having a simulated return loss of - 10.6 dB, - 25.8 dB and - 42.6 dB respectively. In another research work, the design and simulation of a compact dual-band microstrip patch antenna for WiMAX and Wi-Fi applications was presented [14]. The author focused on achieving an improved gain and polarization purity. The antenna was designed using RT /duroid substrate having a 10.2 dielectric constant. The method employed truncated edges and offset feeding process with operating frequencies at 3.65 GHz and 5.42 GHz. the simulated result shows a return loss of – 24.6 dB and -25.6 dB having a peak directivity and gain of 4.92 dBi and 4.51 dBi. A dual-band was achieved for different applications.

3. Methodology

This part of the study provides an insight into the analysis of the mathematical model employed and the impedance matching criterion associated with the process of attaining the DPF of the E-patch microstrip patch antenna.

The presence of the parallel symmetrically slit cut at the boundaries of the microstrip antenna equally acts as a slot; loading them on the patch also alters the Characteristic Mode (CM) [8]. The created slots are incorporated to perturb the flow of current which introduces reactive load distribution to the antenna structure and by varying them influences the behavior of the eigenvalue and the current distribution. This gives rise to a series equivalence inductive and capacitive load to the patch input impedance when in close proximity to the probe feed. The equivalent capacitance counteracts the introduced inductive part giving rise to a second-order mode.

Looking into the analysis of reactive loading it is possible to generalize the eigenvalue problem considering the operator Z as described by Eq. (25):

$$(Z)(j_n) = v_n(W)(j_n) \tag{25}$$

Where Z, j_n, v_n and W is characterized by impedance operator, eigenvector, eigenvalue and the weighing operator. Once W is known, it is possible to solve the eigenvalue problem which is characterized by Eq. (26):

$$(Z)(j_n) = v_n(j_n) \tag{26}$$

The eigenvectors and eigenvalues are complex since (Z) is symmetric on the patch surface. Hence, it is likely to consider the (R) operator as the weighting function, which makes Eq. (27) the new eigenvalue problem.

$$(Z)(j_n) = v_n(R)(j_n) \tag{27}$$

By expanding the Z operator and substituting Z = $R + jX$, $v_n = 1 + j\lambda_n$, Eqs. (28), (29) and (30) are obtained, where λ_n represents the n^{th} eigenvalue.

$$(R + jX)(j_n) = (1 + j\lambda_n)(R)(j_n) \tag{28}$$

$$(R + j[X])(j_n) = ([R][j_n] + j\lambda_n)(R)(j_n) \tag{29}$$

The eigenvalue weighted problem is then gotten by canceling out the like terms:

$$(X)(j_n) = \lambda_n(R)(j_n) \tag{30}$$

Hence, by slot perturbing the PEC surface of the patch, there is an induction of a reactive load distribution to the antenna structure and this influences Eq. (31):

$$[X + X_L][j_n] = \lambda_n[R][j_n] \tag{31}$$

A new λ_n is the n^{th} eigenvalue of the loaded system, which is further simplified to get Eq. (32):

$$\mu_n = (\lambda_n)[\frac{X_L}{R}] \tag{32}$$

Eq. (32) can be inductive or capacitive, and it is apparent that the reactive load effect on the patch surface affects the behavior of the eigenvalue and the current distribution. The resonant frequencies of the CM can now be controlled for values of λ, and when they are being increased or decreased. Subsequently, the impedance equivalent circuit of a parallel RLC Network is as described by Eqs. (33), (34), (35), (36), (37) and (38). Since the impedance Z is frequency-dependent it has both magnitude and phase. Also, Z behaves similarly to a resistor R when combined in series or parallel. Where $Z_{eq,}$ represents the parallel equivalence of $Z_{R,}$ $Z_{L,}$ Z_c identified as the impedance of resistor, impedance of inductor and capacitor [15].

$$\frac{1}{Z_{eq}} = \frac{1}{Z_R} + \frac{1}{Z_L} + \frac{1}{Z_C} \Rightarrow \frac{1}{R} + \frac{J\omega L}{1} + \frac{1}{J\omega C} \tag{33}$$

Since resistors are not dependent on frequency, the voltage and current are in phase hence $Z_R = R$. For inductors in AC the higher the frequency the greater the impedance which results in a current lag over the voltage across by 90^o. On the other hand, capacitors in AC has a low impedance at higher frequencies because the current through the capacitor leads the voltage by 90^o therefore $Z_C = \frac{1}{J\omega C}$.

$$Z_{eq} = Z_R \| Z_L \| Z_C \Rightarrow R \| J\omega L \| \frac{1}{J\omega C} \tag{34}$$

$$Z_{eq} = \frac{Z_R Z_L Z_C}{Z_R Z_L + Z_L Z_C + Z_R Z_C} \Rightarrow \frac{R(J\omega L)(\frac{1}{J\omega C})}{R(J\omega L) + J\omega L(\frac{1}{J\omega C}) + R(\frac{1}{J\omega C})} \tag{35}$$

$$Z_{eq} = \frac{R(J\omega L)(\frac{-1}{\omega C})}{R(J\omega L) + J\omega L(\frac{-1}{\omega C}) + R(\frac{-1}{\omega C})} = \frac{\frac{RL}{C}}{\frac{L}{C} + JR(\omega L - \frac{1}{\omega C})} \tag{36}$$

From this point, Eq. (37) is multiplied by c to eliminate fractions

$$Z_{eq} = \frac{(\frac{RL}{C})(\omega C)}{\frac{L}{C} + JR(\omega L - \frac{1}{\omega C})(wC)} \tag{37}$$

$$Z_{eq} = \frac{R\omega L}{R(1 - LC\omega^2) + JL\omega} \tag{38}$$

Hence Eq. 38 is the resulting equivalent impedance of a single RLC circuit. Hence, a dual band antenna is achieved when quite a number of resonances are adjacent to each other. This is represented in Foster canonical impedance form, where the parallel RLC cells are connected in series $Z_e(S)$ represents the equivalent driving point transfer function as described by Eq. (39):

$$Z_e(S) = JL_p s + \frac{jRL_1 s}{R(1 - L_1 C_1 s^2) + jL_1 s} + \frac{jRL_2 s}{R(1 - L_2 C_2 s^2) + jL_2 s} \tag{39}$$

Hence, these parameters ($L_p, R, L_1, C_1, L_2, C_2$) are calculated using the iterative method to achieve an optimal impedance match.

Figure 3(a) shows the geometric effect and the equivalent circuit of the radiating patch antenna, categorizing the frequency region domain. Figure 3(b) shows the equivalent Foster canonical impedance circuit which depicts the effect of the perturbed patch.

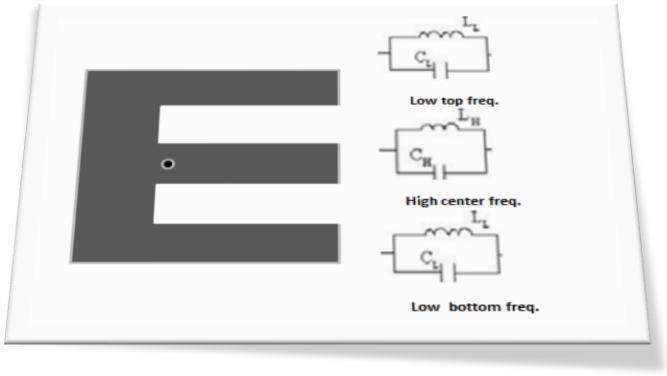

(a)

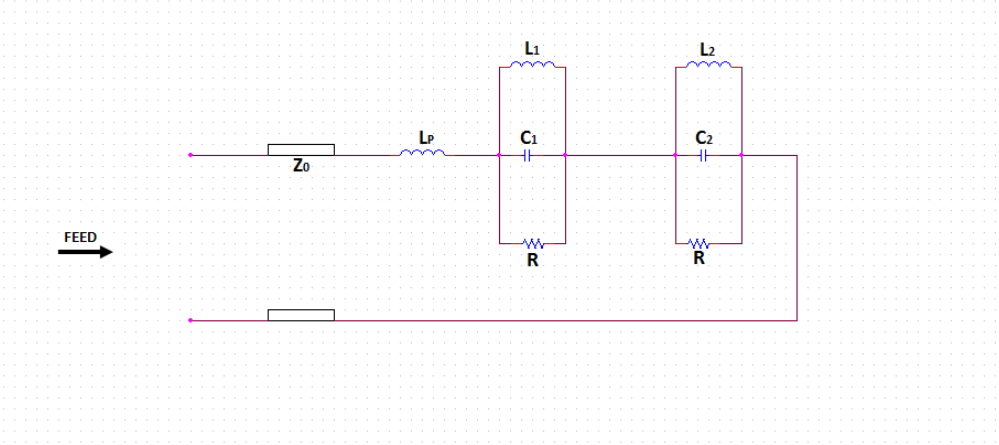

(b)

Fig. 3. (a): The E-patch equivalent circuit, (b): The equivalent Foster canonical impedance circuit

4. Result and Discussion

Figure 4 shows several structural modifications of the E-patch which result in determining the performance of the return loss and the impedance bandwidth. The antenna parameters were synthesized using the full-wave method because the numerical analysis of the problem provides the most accurate solution for the radiation and the impedance matching. Some parametric changes were introduced to the initially designed antenna to achieve the mentioned output.

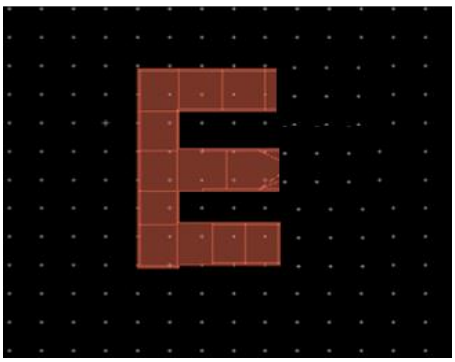

Case (a)

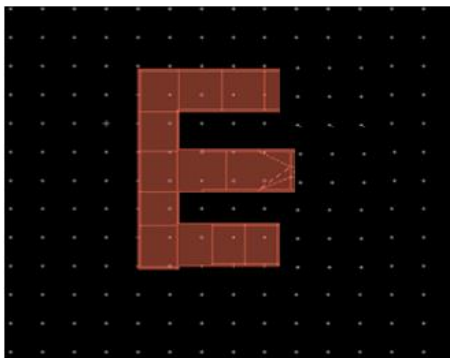

Case (b)

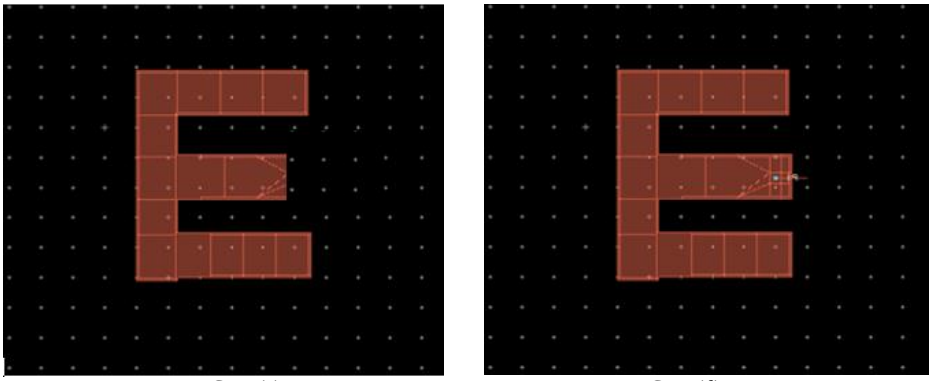

Case (c) Case (d)

Fig. 4. Several Structural modifications of the E-patch

The parametric analysis in figure 5 employed the TML mathematical approach to obtain the arbitrary design parameters. The results show the return loss versus frequency magnitude for several cases of the modified E-patch microstrip antenna.

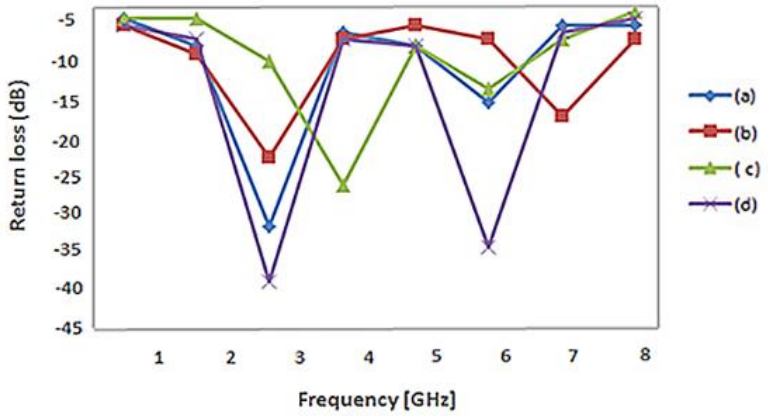

Fig. 5. Return Loss versus Frequency for various parameters

Table 1. Various parameters and effects

Patch	(a)	(b)	(c)	(d)
Slot Width (W_s)	4.46mm	4.46mm	4.25mm	4.25mm
Slot Length (L_1)	12.53 mm	14.60mm	14.60mm	13.92mm
Resonant point	2.4 GHZ, 5.8 GHz	2.4 GHZ, 6.1 GHz	2.6 GHz, 5.8 GHz	2.4 GHz, 5.8 GHz
Return loss	-32 dB, - 14 dB	- 22 dB, - 16 dB	- 26 dB, - 12 dB	-40 dB, - 35 dB
Comment	Non-optimal resonance	Miss resonance	Miss resonance	Optimal resonance

Patch (d) as presented in Table 1 is the proposed antenna optimal parametric result. This plot result shows the performance characteristics as presented by Figure 6 which shows the result of the return loss (S_{11}) plot versus frequency at 2.4 GHz and 5.8 GHz. From the S_{11} parameter variation plot, it is observed that the lower frequency band resonates at 2.4 GHz with a return loss of - 40 dB, while the upper-frequency band resonates at 5.8 GHz with a return loss of - 35 dB. Also, the antenna fractional bandwidth is not less than 10%. The lower the return loss value, the better the performance of the antenna in terms of radiation.

Figure 7 shows the VSWR plot for the resonant frequencies at 2.4 GHz and 5.8 GHz. The return loss is related to the VSWR which shows a variation plot value of 1.020 at 2.4 GHz and 1.036 at 5.8 GHz. This is an acceptable result as a VSWR value greater than 2 usually results in antenna performance degradation. By inspecting the reflected S_{11} magnitude results, about 2.8 % of the signal goes back to the source and 97.2% of the input signal is successfully accepted at the port terminal, while a value of 0.027 was employed to determine the load impedance, whose value is 52.774Ω. The phase plot for these frequencies is presented in Figure 8.

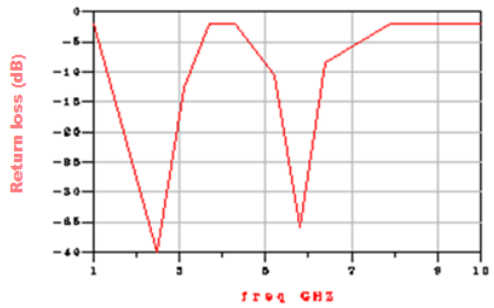

Fig. 6. S_{11} magnitude Versus frequency

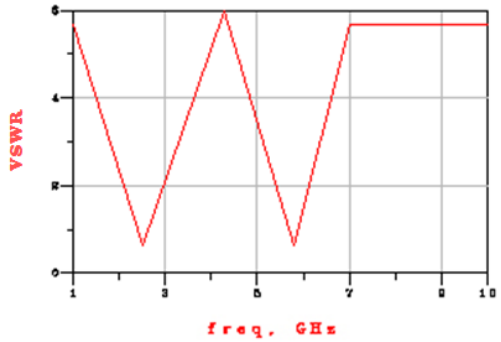

Fig. 7. VSWR result plot versus the frequency

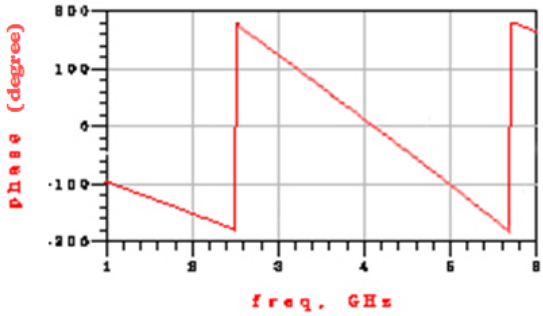

Fig. 8. The S_{11} phase (degree) versus the frequency

Figure 9 shows the axial ratio plot with theta peak point above 10 dB. This implies that the antenna is not purely circularly polarized. The deviation from the circularly polarized field is 3 dB away; this generally means that the antenna fields are not pure linearly polarized either but rather have a mixed polarization (i.e. elliptical) effect. Figure 10 shows the directivity and gain plot and based on this study, the theta peak directivity is 7.4 dBi. It also reveals a peak antenna gain of 3 dBi which is capable of covering a distance of about 140 m.

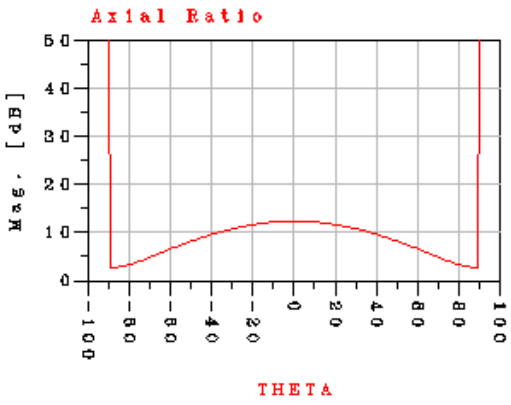

Fig. 9. The axial ratio magnitude Versus theta plot

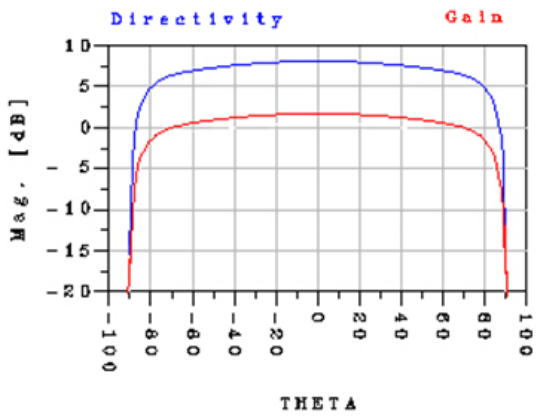

Fig. 10. The directivity and gain magnitude versus theta plot

Figure 11 shows the 3-dimensional view of the electrical field distribution on the surface of the patch. The antenna radiates simultaneously and strongly at both 2.4 and 5.8 GHz as the current density is high at the patch mid-region that is close to the perturbed start point. Figure 12 shows the normalized 3-D radiation of the E-patch antenna far field.

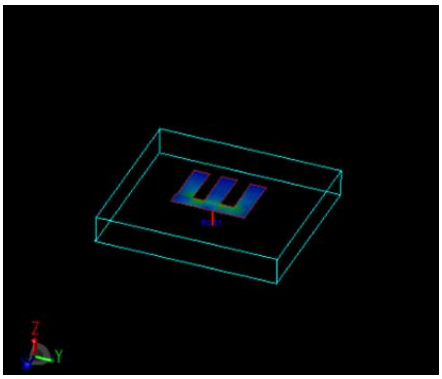

Fig. 11. 3D view of electrical field distribution

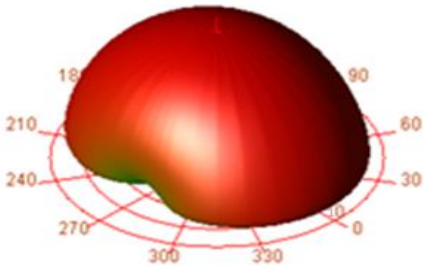

Fig. 12. Normalized 3D radiation far field pattern

5. Conclusion

The Advanced Design System (ADS) Full-wave simulation tool converts the design into a mesh, which computes numerically utilizing MOM based on the size of MSA and boundary condition. After the segmentation, FEM was employed to compute the electrical behavior, EM wave distribution, which in turn calculates the radiation pattern, return loss, axial ratio, VSWR and other related parameters. This work presented an in-depth emphasis into the ADS CAD EM full wave numerical analysis process, and this involved several theories such as the foster reactance, eigenvalue and eigenvector which are all in connection to the microstrip patch antenna modus operandi. The theory of characteristic mode was based on eigenvalue and its effect of perturbing the PEC surface of the patch. This introduces reactive load distribution to the antenna structure, and this influences the behavior of the eigenvalue and the current distribution. The antenna transfer function model was represented through a Foster canonical impedance form, where the parallel RLC cells were connected in series. This driving point function was later modified during simulation by the

method of iteration to attain a better impedance match. The results obtained are based on the performance of the simulated model carried out by ADS. Also, the structural modification method was used to attain the best parametric result, i.e. the minimum reflection coefficient. This study found that the effect of changing the slot length and the width affects the overall frequency response.

References

[1] Arora, A. Rana, A. Yadav, A. and Yadava, R.L. (2021). Design of Microstrip Patch Antenna 2.4 GHz for Wi-Fi and Bluetooth Applications. *Journal of Physics: Conference Series.* 1921(2021) 012023.

[2] Huang, Y. and Boyle, K. (2008). *Antennas from Theory to Practice*. 1st Edition, John Wiley & Sons Ltd. *The Atium, Southern Gates, Chivhester, West Sussex United Kingdom.*

[3] Abdullahi, S.B.M. Shahanawaz, K. Ain M.F. and Zainal. A.A. (2019). Microstrip Patch Antenna: A Review and the Current State of the Art. *Journal of Advanced Research in Dynamical and Control Systems*. 11(7): 510-524.

[4] Anuj, M. (2015). Microstrip Antenna. International Journal of Scientific & Technology Research. 4(3): 54-57.

[5] Sharma, S. Tripathi, C.C. and Rishi, R. (2017). Impedance Matching Techniques for Microstrip Patch Antennas. *Indian Journal of Science and Technology*, 10(28): 1-16.

[6] Rouphael, T. J. (2014). *Wireless Receiver Architectures and Design.* Antenna, RF, Synthesizer, Mixed Signal, and Digital Signal Processing. 1st Edition.

[7] Elrashidi, A. Elleithy, K. and Bajwa, H. (2011). The Fringing Field and Resonance Frequency of Cylindrical Microstrip Printed Antenna as a Function of Curvature. *Article published by University of Bridgeport, USA.* 3(2): 1-12.

[8] Xu, J. Shen, D.Y. Wang, G.H. Zhang, X.H. Zhang, X.P. and Wu, K . (2012). A Small UWB Antenna with Dual Band Notched Characteristics. *International Journal of Antennas and Propagation.*

[9] Rahola, J. (2007). Characteristic Mode Analysis: Eigenvalue Analysis of Antenna Structure, Nokia Z Research Center. [Online] Available at: https://cerfacs.fr/wp-content/uploads/2016/03/rahola.pdf. [Accessed 2018].

[10] Geyi, W. Jarmuszewski, P. and Qi Y. (2000). The Foster Reactance Theorem for Antenna and Radiation Q. *IEEE Transactions on Antennas and Propagation.* 48(3): 401-408.

[11] Saturday, J.C. Udofi, K.M. and Obot, A.B. (2016). Compact Rectangular Slot Patch Antenna for Dual Frequency Operation using Inset Feed Technique. *International Journal of Information and Communication Science*. 1(3): 47-53.

[12] Keshav, Pandey, R. Garg, M. and Mamta (2019). Analysis of Compact Multi-band and Ultra-Wide Band Rectangular Microstrip Patch Antenna for S, C and X Band Frequency Ranges. *International Journal of Research in Engineering, Science and Management*, 2(5): 489-493.

[13] Abdul, R.Z. and Sheriff, O. (2018). The Modeling and Simulation of a Rectangular Microstrip Antenna. *International Journal of Engineering and Emerging Science Discovery*. 3(2): 58-68.

[14] Haruna, Y.S. (2019). Design and Simulation of Compact Dual Band Microstrip Patch Antenna for WiMAX and Wi-Fi Applications. International *Journal of Engineering Technology Creativity and Innovation*. 2(1): 1-13.

[15] Bumm, L.A. Retrieved (2019). AC Steady-state Circuits, AC Impedance, RC, RL & RLC Filters: An article published by Creative Commons Attribution (Phys). [Online] Available at: http://www.nhn.ou.edu/~bumm/ELAB/Lect_Notes/AC_impedance_v2_1_1.html.n

Authors' Profiles

Dr. Fubara E. Alfred-Abam was born in April 1988 and hails from Okrika Rivers State Nigeria. He received his BEng. Degree in Electrical and Electronics Engineering from the University of East London (UEL) in 2013, afterward pursued an MSc in Computer Systems Engineering from (UEL) in 2015. He obtained his Ph.D. in Electrical and Electronics Engineering from Bells University in 2021. He is vastly Knowledgeable in the areas of Electronics & Communication, Computer Networking, and Electrical Power systems. He currently works as a Lead Research and Development Engineer for EKEDC, Nigeria. His research interest includes Wireless Communication, Antenna & Wave Propagation, Transmission line and Power System Distribution. He has published papers in International Journals and International Conferences.

Gyang Paul Pam was born in Plateau, Nigeria. He received a B.Sc. degree in Electrical and Electronics Engineering from the Federal University of Technology, Owerri, Nigeria in 2015, and is currently an MSc student at the University of Lagos, Akoka, Nigeria. He is a graduate research assistant to his supervisor who is a Postdoctoral Fellow at the Centre for Energy & Electric Power at the Tshwane University of Technology in 2022. Presently, Pam is a Research and Development/Simulation Engineer at Eko Electricity Distribution Company, Lagos. His current research interests lie in the areas of Lumped and Distributed Networks, Integration of Renewable Energy, Energy Harvesters, and Machine Learning Applications in Power System Resilience.

Fiyinfoluwa P. Olubodun was born in Lagos State, Nigeria and comes from Oyo State, Nigeria. He received his B.Tech. Degree in Electrical Engineering (Power Options) from Ladoke Akintola University of Technology in 2015 and thereafter furthered to obtain an M.Eng. Degree in Electrical and Electronics Engineering from Federal University of Technology in 2019. Fiyin is a meritorious power systems scholar and skilled in data analysis, python, MATLAB and various electrical testing equipment. He is a pioneer member of the predictive maintenance department in Eko Electricity Distribution Company, Lagos, Nigeria. His research interests are System Stability, Smart Grids, Renewable Energy and Predictive Analysis.

How to cite this paper: Fubara Edmund Alfred-Abam, Pam Paul Gyang, Fiyinfoluwa P. Olubodun, "Full-Wave Numerical Analysis of Dual-Band E-Patch Antenna and Reactive Loading Technique to Ascertain the Impedance Driving Point Function", International Journal of Wireless and Microwave Technologies(IJWMT), Vol.13, No.3, pp. 26-38, 2023. DOI:10.5815/ijwmt.2023.03.03